Research Article

Siyi Chen[#], Shuang Yang[#], Sisi Chen, Fang Zuo, Pan Wang, Ying Li, and Yong You*

Polyarylene ether nitrile dielectric films modified by HNTs@PDA hybrids for high-temperature resistant organic electronics field

https://doi.org/10.1515/ntrev-2023-0117 received June 4, 2023; accepted August 12, 2023

Abstract: In this work, mussel-inspired surface functionalization of halloysite nanotubes (HNTs) were coated by in situ self-polymerization of polydopamine (PDA) to synthesize core-shell structural composites (HNTs@PDA), and then incorporated into polyarylene ether nitrile (PEN) matrix. Due to the strong adhesion of the PDA modification layer and the formation of hydrogen bonds between the polar nitrile group of PEN and the catechol group of PDA, the dispersion and interfacial compatibility of HNTs@PDA in the PEN matrix are improved. The results show that the dielectric constant of PEN/HNTs@PDA 20 nanocomposites reaches 11.56 (1 kHz), which is 3.2 times that of pure PEN. In addition, after heat treatment, a chemical cross-linking reaction occurred between the PEN matrix to form a cross-linked PEN (CPEN) based nanocomposites, which further improved the thermal stability of the nanocomposites. The results show that the $T_{\rm g}$ of CPEN/HNTs@PDA 20 nanocomposites reaches 215.5°C, which is 47.7°C higher

These authors contributed equally to this work and should be considered first co-authors.

than that of PEN/HNTs@PDA 20. Moreover, the dielectric constant-temperature coefficient of all CPEN nanocomposites is less than 7×10^{-4} °C⁻¹ at the temperature range of 25–180°C. All in all, this work provides a simple and environmentally friendly strategy to adjust the dielectric properties of polymer-based ceramic nanocomposites, which provides a pathway for its application as a dielectric material in the film capacitors field.

Keywords: polyarylene ether nitrile, nanocomposites, dielectric properties, core-shell structure

1 Introduction

In recent years, polymer-based nanocomposites with outstanding dielectric properties and high temperature resistance have received increasing attention due to the widespread demand in the electronic device fields [1]. Although the traditional inorganic ceramic dielectrics are widely used owing to their high dielectric constant, their inherent characteristics of heavy weight, difficult processing, and brittleness are no longer sufficient for the current practical application. In comparison, polymeric materials have exhibited the advantages of lightweight and flexibility, but their low dielectric constant also limits their application to a great extent. Therefore, combining the two-component materials is an effective way to overcome these limitations. Therefore, polymer/ceramic-filler dielectric nanocomposites have become a significant research direction for energy storage field due to its combination of high insulation, high mechanical strength, and easy processing, as well as the great high dielectric constant and stable thermal stability [2].

Nowadays, ceramic nanomaterials, such as $BaTiO_3$ and TiO_2 [3], are commonly used in the preparation of high dielectric polymer nanocomposites. Among these nanofillers, halloysite nanotubes (HNTs), consisting of a natural bilayer structure of silica-aluminate [4], is a one-dimensional tubular ceramic material with excellent mechanical strength and thermal stability. HNTs have many advantages

^{*} Corresponding author: Yong You, Key Laboratory of General Chemistry of the National Ethnic Affairs Commission, School of Chemistry and Environment, Southwest Minzu University, Chengdu 610041, China; Key Laboratory of Pollution Control Chemistry and Environmental Functional Materials for Qinghai-Tibet Plateau of the National Ethnic Affairs Commission, School of Chemistry and Environment, Southwest Minzu University, Chengdu 610041, China, e-mail: youyong@swun.edu.cn Siyi Chen, Shuang Yang, Sisi Chen, Fang Zuo: Key Laboratory of General Chemistry of the National Ethnic Affairs Commission, School of Chemistry and Environment, Southwest Minzu University, Chengdu 610041, China; Key Laboratory of Pollution Control Chemistry and Environmental Functional Materials for Qinghai-Tibet Plateau of the National Ethnic Affairs Commission, School of Chemistry and Environment, Southwest Minzu University, Chengdu 610041, China Pan Wang, Ying Li: School of Mechanical Engineering, Chengdu University, Chengdu 610106, China

in applications due to their structure similar to that of carbon nanotubes (CNTs) [5–7]. On the one hand, HNTs are abundant in source, inexpensive, non-toxic and non-hazardous, and has good biocompatibility. On the other hand, HNTs have fewer functional groups on its surface and less π – π interactions between nanotubes, enabling easier dispersion in matrix polymer resin. Consequently, HNTs offer a viable alternative to the more expensive CNTs in polymer nanocomposites and multifunctional nanocomposites.

Polyarylene ether nitrile (PEN) [8,9], as a new class of high-performance and high-temperature resistant special engineering plastics, has received wide attention for its good processing properties, outstanding thermal stability, and tensile strength. It is because of a large number of benzene rings in the backbone of the PEN molecule, which makes the molecular chain segments have high mechanical strength. The presence of the strong polar side group nitrile makes PEN have a dielectric constant between 3.8 and 6.0 [10]. Additionally, PEN exhibits high temperature and corrosion resistance, expanding its applications across various industries. However, similar to many polymers, their relatively low dielectric constants and energy storage densities make it difficult to meet the current practical applications. Despite extensive research on dielectric nanocomposites based on materials such as GO, HNTs, and BaTiO₃ [11-13], their dielectric losses remain at elevated level. Hence, further exploration is necessary to devise high-performance polymer-based nanocomposites.

As we are aware, the interface compatibility between the matrix and the nanofiller plays a crucial role in the preparation of polymer-based nanocomposites with exceptional comprehensive properties. Inadequate interfacial compatibility can result in nanofiller aggregation within the matrix, leading to high dielectric loss. Therefore, it is essential to introduce a simple and effective method for nanoparticle surface modification needs to be introduced. Recently, dopamine (DA) has often been used by researchers as a surface modification material for nanomaterials owing to its abundant hydroxyl functional groups and good adhesion properties on its surface [14,15]. In addition, DA can also form polydopamine (PDA) by *in situ* self-polymerization under certain conditions [16]. It can effectively improve the interfacial compatibility.

In this work, PEN/HNTs@PDA one-dimensional nanotube composite films were designed. Initially, the HNTs were first coated with a PDA organic layer, which offers abundant surface hydroxyl groups. Subsequently, different mass fractions of HNTs@PDA were introduced into PEN for preparing PEN/HNTs@PDA nanocomposites. Finally, the dielectric, mechanical, and thermal properties of PEN/HNTs@PDA composite films are studied in detail, and the

influence of interface compatibility between HNTs@PDA and PEN matrix on the structure and properties of composite films is further explored, which provides a new way for the preparation of polymer nanocomposites with excellent comprehensive properties.

2 Experimental methods

2.1 Materials

HNTs (AR) was provided from Guangzhou Worun Material Technology Co., Ltd (China); Dopamine hydrochloride (98%) was purchased from Chengdu Best Reagent Co., Ltd (China). Tris(hydroxymethyl) aminomethane (99.9%), concentrated hydrochloric acid (HCl, AR), and *N*-methyl-2-pyrrolidone (NMP, 98%) were purchased from Kelong Reagent Co., Ltd, Chengdu, China. The PEN was synthesized in the laboratory. All materials were used without further purification.

2.2 Preparation of PEN composite dielectric films

The core-shell structure of the PDA interface functionalized HNTs were prepared through *in situ* self-polymerization of DA, and the corresponding preparation mechanism diagram is shown in Figure 1. First, HNTs (0.40 g) were dispersed into Tris-HCl buffer solution (200 mL) with ultrasonic stirring. Then, dopamine hydrochloride (0.20 g) was added to the system and continued the stirring reaction for 4 h. The products were repeatedly washed with deionized water to neutral, and dried at 50°C overnight to obtain HNTs@PDA hybrids.

PEN was synthesized in the laboratory following the procedures outlined in the literature [17], and its structure is presented in Figure S1. The PEN nanocomposites were prepared by solution casting method. The specific steps are as follows: first, a certain mass of HNTs@PDA hybrids was placed in NMP solvent and dispersed by ultrasonic waves for 1 h, then the corresponding mass of PEN powder was added and heated at 200°C for 2 h until the PEN is completely dissolved. After that, the solution of PEN/HNTs@PDA was slowly poured onto a horizontally placed glass plate with the procedure of 80/100/120/160°C for 1 h and 200°C for 2 h, respectively. Finally, after natural cooling to room temperature, the PEN/HNTs@PDA composite film was obtained. The PEN nanocomposites with HNTs@PDA mass fractions of 0/5/10/15/20 wt%, which were named as PEN, PEN/HNTs@PDA 5,

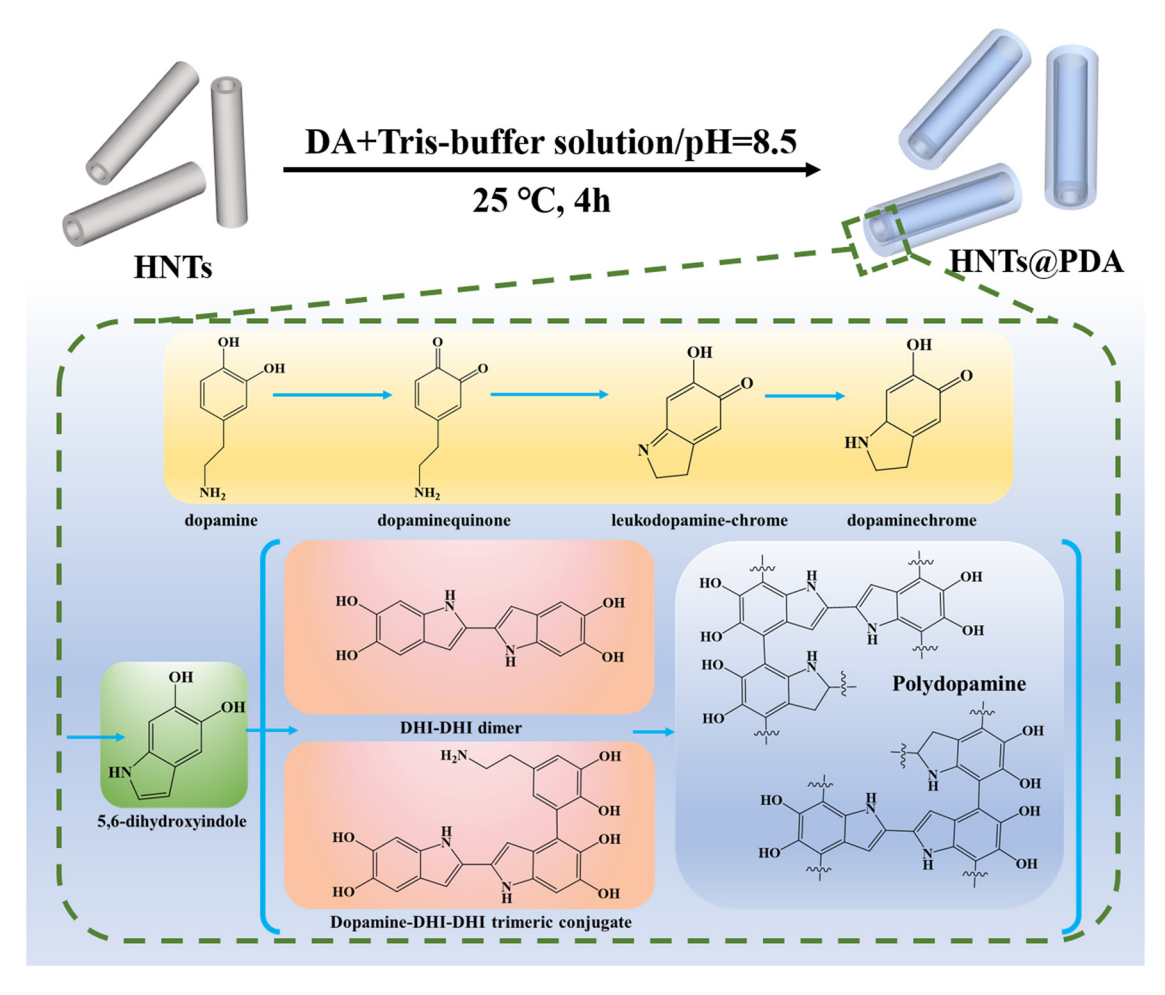


Figure 1: Schematic diagram of the preparation of HNTs@PDA hybrids.

PEN/HNTs@PDA 10, PEN/HNTs@PDA 15, and PEN/ HNTs@PDA 20. Additionally, the composite films with HNTs mass fraction of 5/10/15/20 wt% were prepared and named as PEN/HNTs 5, PEN/HNTs 10, PEN/HNTs 15, and PEN/HNTs 20.

The above PEN/HNTs@PDA nanocomposites were placed in a high temperature oven at 320°C for 4 h. After natural cooling, the composite films were detached from the glass plates and labeled as cross-linked PEN (CPEN), CPEN/ HNTs@PDA 5, CPEN/HNTs@PDA 10, CPEN/HNTs@PDA 15, and CPEN/HNTs@PDA 20.

2.3 Characterization

Fourier-transform infrared (FTIR, Thermo Nicolet, IR 200) spectra were obtained in the attenuated total reflectance mode from 400-4,000 cm⁻¹. The X-ray diffraction (XRD, Beijing Pu-Analysis General Instrument, XD-6, 4°/min) analysis was tested at a range of 5°-85°. UV-vis spectroscopy

(UV-500, Thermo Nicolet) was tested at 200-900 nm. Zeta potential of the nanotubes was tested by using a zetasizer instrument (Nano zs, Malvern, USA). Each sample was measured three times to ensure repeatability. The microscopic morphology images were tested by SEM (JEOL JSM-5900LV, Tokyo, Japan) and TEM (JEOL JEM-F20, Tokyo, Japan). Mechanical properties were tested on electromechanical universal testing machine (QX-W200, Shanghai Qixiang Testing Instrument Co., Ltd), the tensile rate is 5 mm/min. Differential scanning calorimetry (DSC, TA, Q2000, 10°C/min) was used to investigate the change in glass transition temperature of the polymer films, which were tested in an atmosphere of N₂ over a range of 50-400°C. The thermal stability of the materials was characterized by thermogravimetric analysis (TGA, TA, Q50, 20°C/min) over the range of 25-800°C. Dielectric properties were measured by a TH2819A LCR meter (Tonghui Electronics Co., Ltd, China) from 100 Hz to1 MHz. The heat transfer properties were analyzed using Infrared thermal imager (FLIR Systems Inc, NASDAQ: FLIR).

3 Results and discussion

3.1 Structural characterization of HNTs@PDA

The FTIR spectra of HNTs and HNTs@PDA are shown in Figure 2(a). Among them, the characteristic peaks observed at 3,716 and 3,635 cm⁻¹ belongs to the stretching vibration of Al-OH, the characteristic peak at 1,037 cm⁻¹ is mainly caused by the stretching vibration of Si–O group in HNTs. Additionally, peak at 917 cm⁻¹ indicates the bending vibration of Al-OH and another bending vibration peak of Al-O-Si at 517 cm⁻¹. These peaks confirm the presence of these respective groups in HNTs [18]. Besides, the peak appearing at 3,444 cm⁻¹ on the curve of HNTs@PDA is the stretching vibration of –OH and –N–H in PDA. For the absorption

peak at 1,627 cm⁻¹, it is the peak of –N–H bending vibration in PDA. And the characteristic peaks located at 1,508 and 1,290 cm⁻¹ are the peaks of the stretching vibration of the C–C group on the benzene ring and the characteristic absorption peak of the phenolic hydroxyl group in PDA, respectively [19,20]. Therefore, the result can prove that HNTs are successfully modified by PDA.

Figure 2(b) shows the XRD diffraction spectra of HNTs and HNTs@PDA. By comparing the PDF standard card (JCPDF#29-1487), it can be seen that pure HNTs have distinct diffraction peaks at $2\theta = 12.1^{\circ}$, 20.1° , 24.6° , 35° , 54.5° , and 62.5° , which represents the presence of (001), (110), (002), (110), (210), and (300) crystal planes in its crystal structure [21]. The result indicates that the crystal structure of the HNTs did not change before and after the PDA coating. Meanwhile, as shown in Figure 2(c), the HNTs, HNTs@PDA as well as DA were tested by UV-Vis

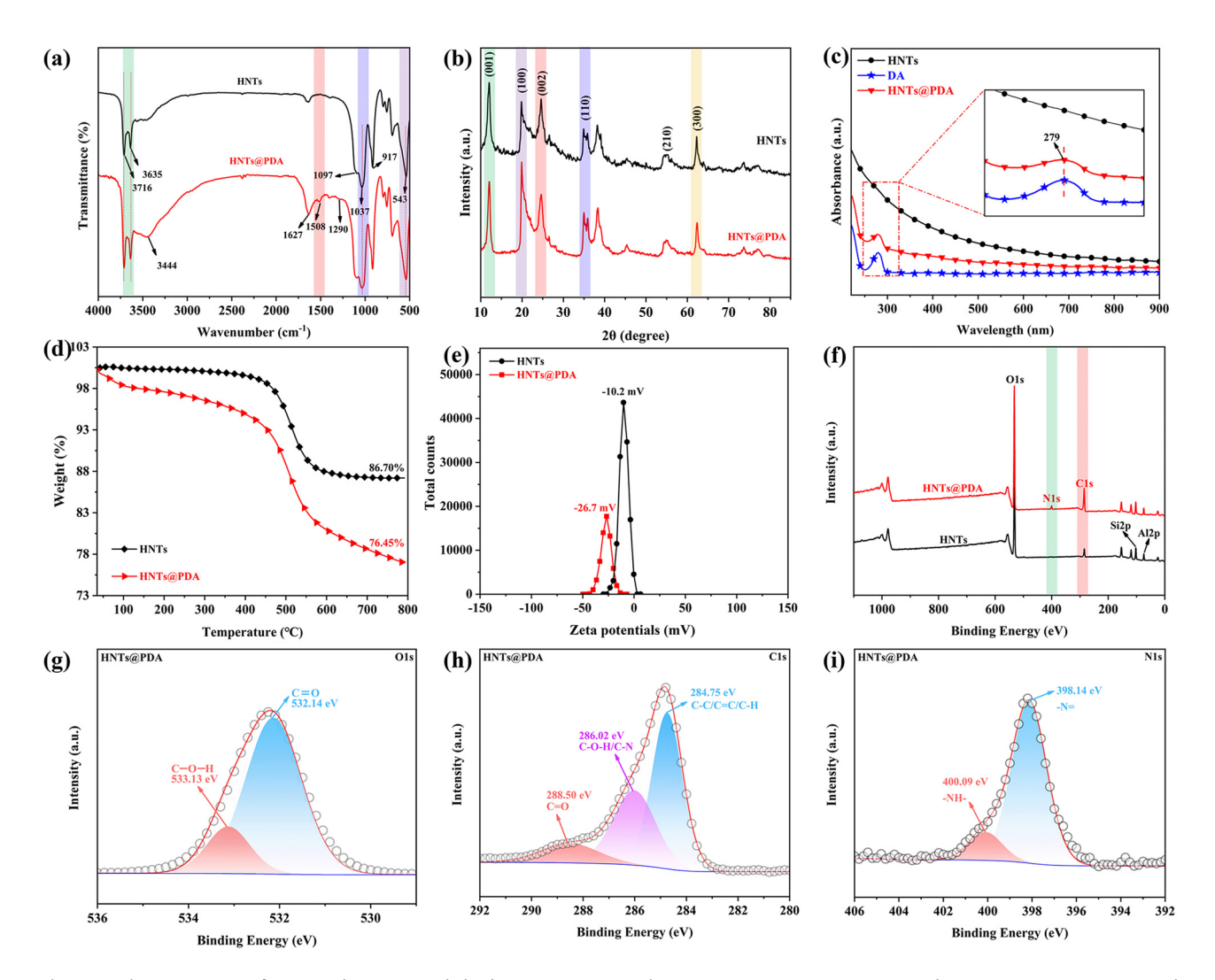


Figure 2: Characterization of HNTs and HNTs@PDA hybrids: (a) FTIR spectra; (b) XRD patterns; (c) UV-vis spectra; (d) TGA curves; (e) zeta potential spectra; (f) XPS survey spectra; (g) O1s, (h) C1s, and (i) N1s XPS spectra of HNTs@PDA.

spectroscopy. The curves of DA and HNTs@PDA both have absorption peaks at about 277 nm, which are mainly the absorption of the benzene ring in the system [22]. This result proves that the PDA is successfully coated on the surface of HNTs. The amount of PDA coating on the surface of functionalized HNTs were investigated by TGA analysis. Figure 2(d) shows the TGA curves of the HNTs before and after modification. It can be seen that the weight loss of HNTs is 13.30% at 800°C, which is mainly due to the decomposition of hydroxyl functional groups (Al-OH) on the surface of HNTs. In contrast, HNTs@PDA has a larger weight loss than that of HNTs in the temperature range of 50–800°C, reaching 23.55%. From the change in weight fraction, it can be estimated that the coating amount of PDA is about 8.6%, which further confirms that the surface of HNTs is successfully coated by PDA. Zeta potential measurements reflect the amount of charge carried by the solid surface. The aqueous solutions of HNTs and HNTs@PDA were characterized by zeta potential, which are shown in Figure 2(e) [22]. It can be seen that both HNTs and HNTs@PDA are negatively charged with zeta potential values of -10.2 and -26.7 mV, respectively. The zeta potential is mainly related to the charge on the surface of the filler, and HNTs exhibit a negative charge due to the hydroxyl group on their surface. In addition, when the DA monomer forms PDA by in situ oxidative self-polymerization, a large number of catechol groups are exposed on its surface,

showing a negative potential. It is once again demonstrated that PDA successfully modifies the surface of HNTs and causes a significant reduction in the zeta potential of the filler [23]. Therefore, the absolute value of the zeta potential of the HNTs@PDA is much larger than that of HNTs, and according to the principle of uniform charge mutual repulsion, the charge repulsion between the HNTs@PDA is much greater than that between the HNTs, which makes the HNTs@PDA hybrids less easy to aggregate and will be better dispersed in the polymer matrix. This result is consistent with the dispersion test of the filler in the NMP solvent.

As shown in Figure S2, the PDA-modified HNTs have excellent dispersion in the NMP solvent, and there is still no obvious agglomeration phenomenon after 48 h, while the pure HNTs settle almost completely due to agglomeration after 1 h in the NMP solvent. This result is due to the fact that a large number of catechol groups are exposed on the surface of the PDA, resulting in a significant increase in the absolute value of the zeta potential of HNTs@PDA. According to the principle of charge repulsion, the repulsion between negative charges makes HNTs@PDA hybrids less prone to agglomeration and better dispersed in NMP.

In Figure 2(f), the XPS spectra of HNTs and HNTs@PDA hybrids are displayed. The HNTs@PDA spectrum reveals a diffraction peak at 400.05 eV for N1s, primarily originating

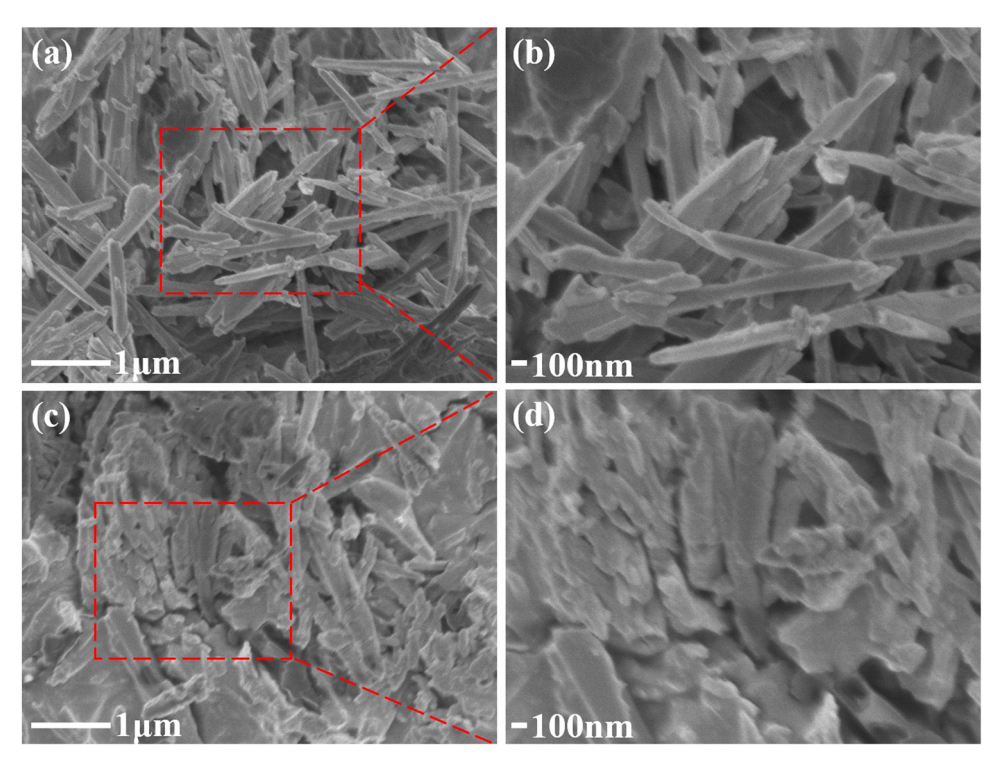


Figure 3: SEM images of functional nanofillers: (a) and (b) HNTs; (c) and (d) HNTs@PDA

from the N element in the PDA of the HNTs@PDA hybrids [24]. Meanwhile, the O1s, C1s, and N1s of the HNTs@PDA exhibit distinctive split peaks. As depicted in Figure 2(g)–(i), the C1s spectra is fitted with three diffraction peaks at 288.50, 286.02, and 284.75 eV, corresponding to the C=O, C-N/C-OH, and C-C/C=C/C-H bonds, respectively [25]. The N1s spectra at 398.14 and 400.09 eV are fitted with two diffraction peaks corresponding to -N= and -NH- bonds, respectively [26]. It indicates that self-polymerization reactions are performed between the DA, which is consistent with the polymerization mechanism proposed in the previous results of FTIR and TGA. It also confirms the successful preparation of PDA-modified layer on the HNTs.

The SEM images of nanofillers are shown in Figure 3. As shown in Figure 3a and b, the HNTs have a one-dimensional tubular structure with smooth outer surface and relatively uniform size. In contrast, the PDA-modified HNTs display varying sizes and rough surfaces (Figure 3c and d), providing further evidence of the attachment of the PDA layer around the HNTs.

The microstructure of HNTs and HNTs@PDA was further assessed using TEM. As shown in Figure 4a and b, the pristine HNTs were tubular with smooth surface and no obvious

ripples and folds. However, following the surface modification of HNTs, the HNTs were enveloped by a thin organic layer (Figure 4c and d), providing further confirmation of the presence of the PDA layer. Furthermore, the elemental mapping images of HNTs@PDA shows that the Al, Si, and O elements are distributed throughout the HNTs, while the C and N elements of the PDA structure cover the whole HNTs and are uniformly distributed (Figure 4e). These visual results also further confirm the successful *in situ* generation of PDA on the surface of HNTs.

3.2 Structure and properties of nanocomposites

The morphologies of PEN- and CPEN-based nanocomposite film were characterized by SEM, respectively. It can be observed from Figure 5(a) that the pure PEN films have smooth cross-sections. Figure 5(b) shows the morphology of PEN/HNTs 20, it is clear that most of HNTs are exposed on the surface of the PEN matrix, and obvious separation and agglomeration between HNTs and PEN matrix is

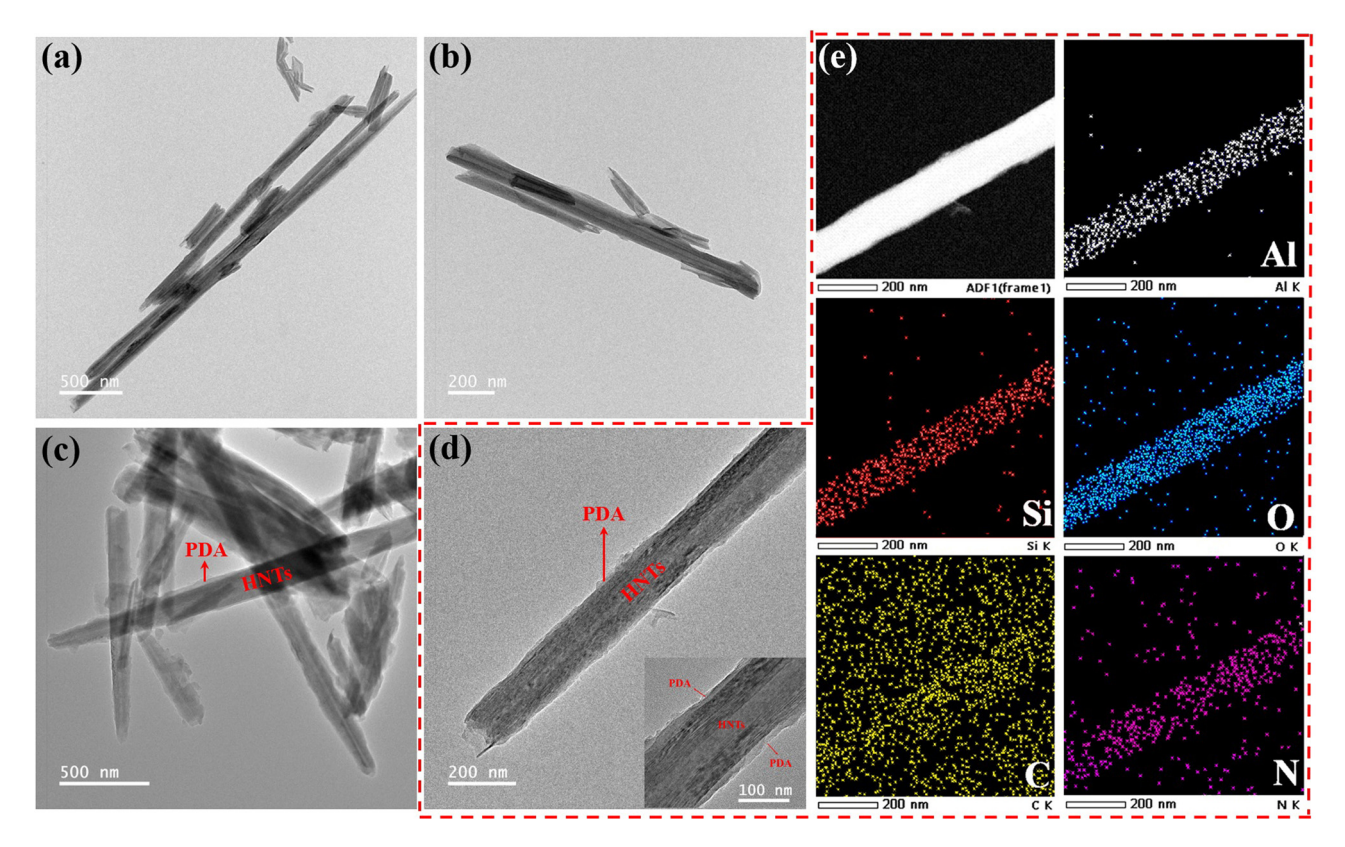


Figure 4: TEM and mapping images of functional nanofillers: (a) and (b) HNTs; (c) and (d) HNTs@PDA; (e) the elemental mapping images of HNTs@PDA.

observed. This is due to the weak interface interaction between HNTs and PEN, which leads to local agglomeration in the PEN matrix. On the contrary, after PDA modification, the HNTs@PDA hybrids are more uniformly distributed in PEN without obvious aggregation, and the HNTs@PDA are all wrapped by the PEN matrix with no obvious HNTs alone in the cross-section (Figure 5(c)). It is mainly attributed to the reduction in the agglomeration of HNTs covered by dopamine self-polymerization [27]. At the same time, as the PDA molecule contains a benzene ring structure similar to that of PEN, the compatibility between them is improved. In addition, the abundant catechol groups on the PDA can react and adhere to the organic polymer, greatly improving the compatibility of the filler with the matrix. Therefore, it can be concluded that PDA-modified HNTs have better dispersion capacity in the PEN matrix [28].

In addition, the nanocomposites after high-temperature heat treatment were also investigated by SEM. The cross-section of all CPEN composite films shows a brittle break, and its surface is much flatter and smoother (Figure 5(a1–c1)), which is due to the fact that the –CN group on the PEN chain is cross-linked at high temperatures, generating a stable triazine ring. After the introduction of HNTs@PDA hybrids, the composite film exhibits excellent interfacial compatibility due to the triazine ring structure formed

by the nitrile groups between the PEN molecular chains, which enhances the interfacial interaction and further improves the compatibility of the HNTs@PDA with the PEN matrix, thereby further reducing the agglomeration of HNTs@PDA hybrids.

To investigate the microstructure of HNTs in the PEN matrix before and after modification, the XRD of the PEN nanocomposites with different filler contents were tested separately, which are shown in Figure 6a. It can be seen from the Figure that all composite films have obvious diffraction peaks at 2θ = 12.2°, 20°, and 24.6°, which are attributed to the (001), (110), and (002) crystal planes of HNTs, respectively [21]. In addition, the XRD tests were also performed on the composite films after heat treatment. As shown in Figure 6b, the structure of CPEN/HNTs@PDA composite films shows a similar phenomenon to that of PEN/HNTs@PDA, and the results show that the crystal structure of the HNTs@PDA remains intact after high-temperature heat treatment, which provides a theoretical basis for the application in high-temperature environments.

The mechanical properties of composite materials are an important index parameter in industrial applications, which affect the value of materials in practical applications. The mechanical properties of PEN/HNTs@PDA films are shown in Figure 7. The results show that the tensile

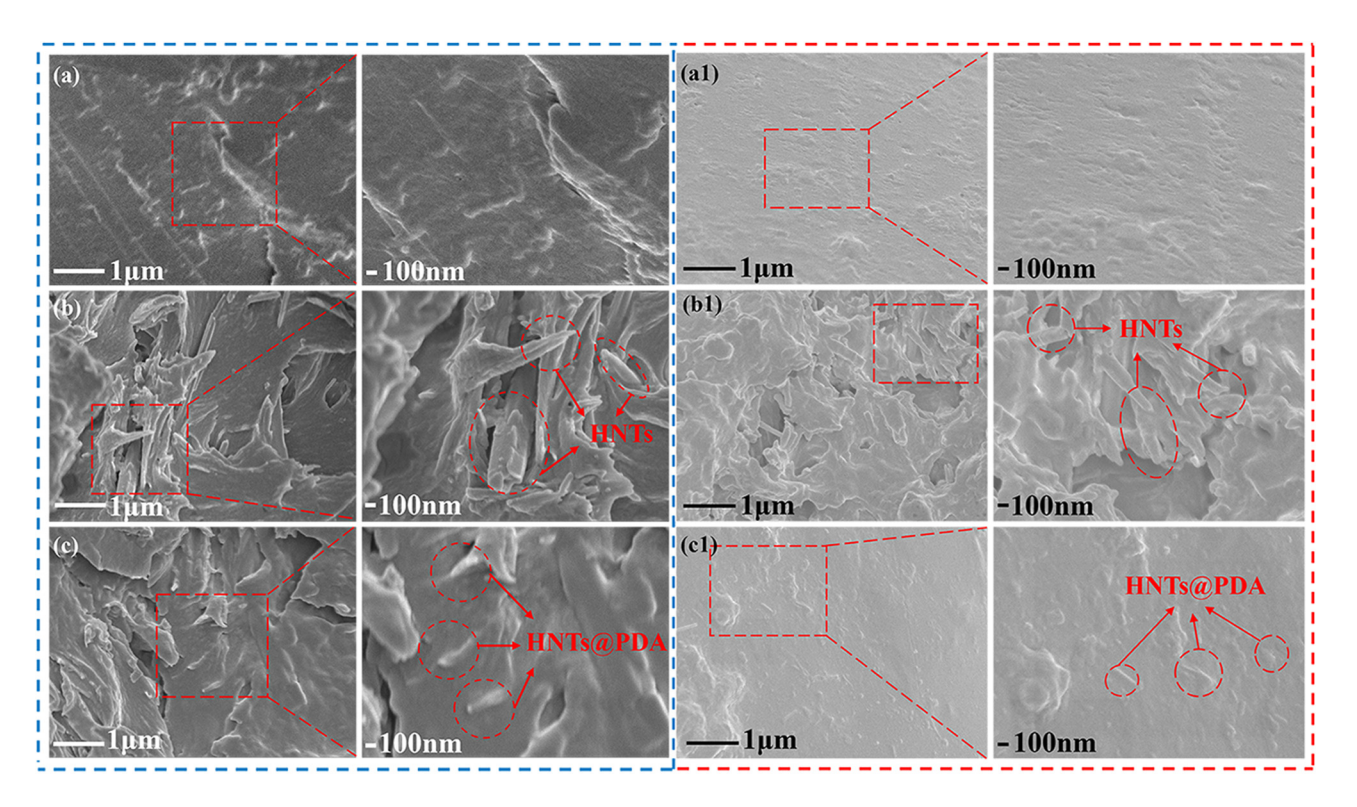


Figure 5: The cross-section SEM images of composite films: (a) PEN; (b) PEN/HNTs 20; (c) PEN/HNTs@PDA 20; (a1) CPEN; (b1) CPEN/HNTs 20; (c1) CPEN/HNTs@PDA 20.

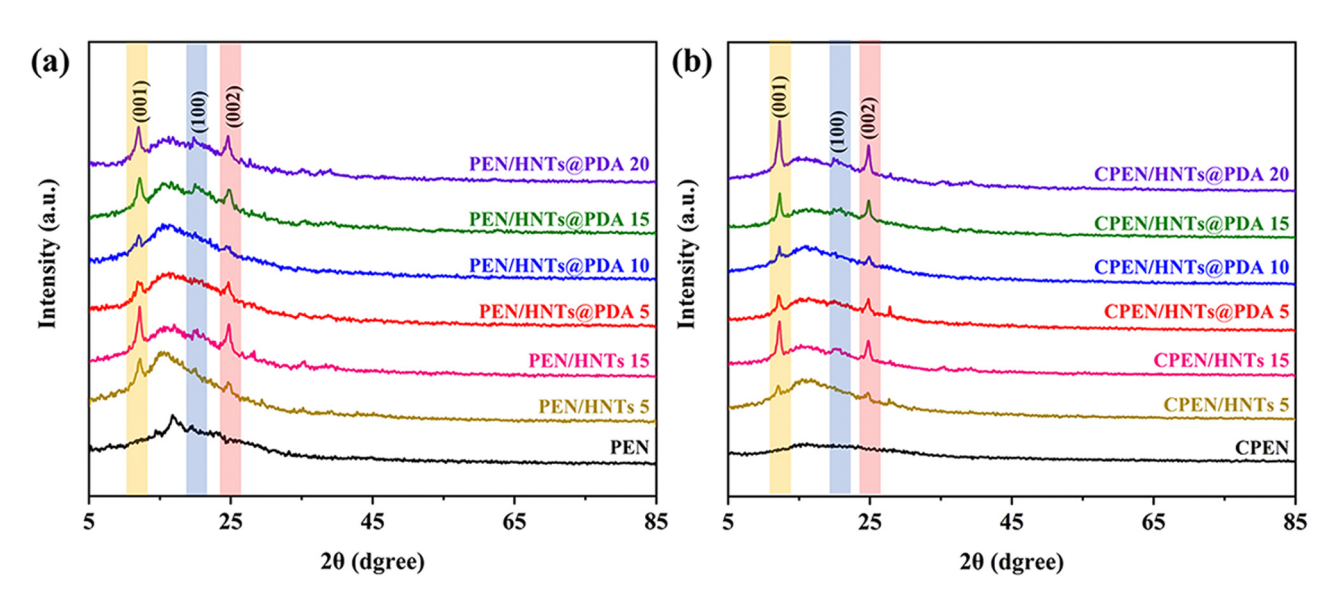


Figure 6: XRD patterns of nanocomposite films: (a) PEN/HNTs@PDA; (b) CPEN/HNTs@PDA.

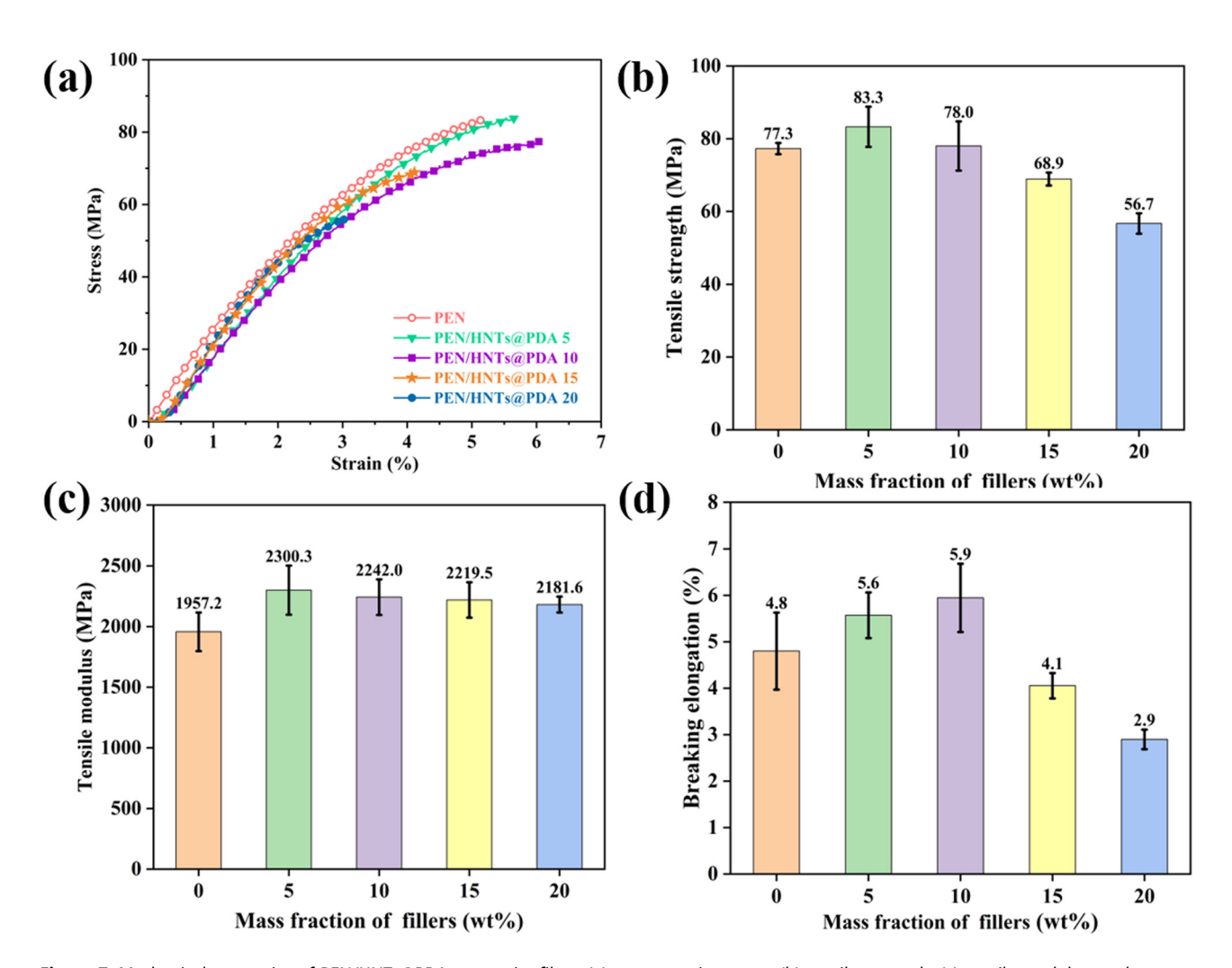


Figure 7: Mechanical properties of PEN/HNTs@PDA composite films: (a) stress–strain curves; (b) tensile strength; (c) tensile modulus; and (d) elongation at break.

strength and modulus of pure PEN is 77.3 and 1957.2 MPa, respectively. However, the incorporation of HNTs@PDA fillers significantly alters the mechanical properties of the PEN composite film, exhibiting an overall trend of initial improvement followed by a decrease. After adding 5 wt% HNTs@PDA filler, the tensile strength and modulus increase to 83.3 and 2300.3 MPa, respectively. After the filler mass fraction exceeded 10 wt%, the tensile strength and modulus of the nanocomposites begin to gradually decrease. The above results are mainly due to the fact that the HNTs@PDA is an inorganic nanotube material with a relatively large length and diameter. When a certain concentration is reached, it can entangle with the PEN molecular chain, forming a physical cross-linking network in the composite system, which can enhance the physical and mechanical meshing between the HNTs@PDA and PEN matrix, thereby hindering the movement of the polymer molecular chain. When the material is subjected to external forces, it is transferred to rigid nanotubes, which will enhance the strength and modulus of the nanocomposites [29]. However,

when the amount of HNTs@PDA filler is added to a certain extent, agglomeration between the HNTs@PDA may inevitably occur, resulting in a decrease in tensile strength and modulus. In addition, the elongation at break of the PEN/HNTs@PDA nanocomposites showed a tendency to increase and then decrease with the increase in the filler content, reaching a maximum value of 5.9%. This is mainly due to the fact that a small amount of HNTs@PDA has good compatibility with PEN and increases the plasticity of the nanocomposites due to the presence of PDA, which increases the elongation at break of the nanocomposites. However, with the further increase in HNTs@PDA content, the agglomeration between the HNTs@PDA may inevitably occur, which leads to a significant decrease in tensile strength, resulting in a rapid decrease in elongation at break. These results indicate that filling with appropriate number of HNTs@PDA fillers can enhance the mechanical properties of nanocomposites.

To further validate the impact of the modified filler on the mechanical properties of nanocomposites, the mechanical properties of PEN/HNTs and PEN/HNTs@PDA were

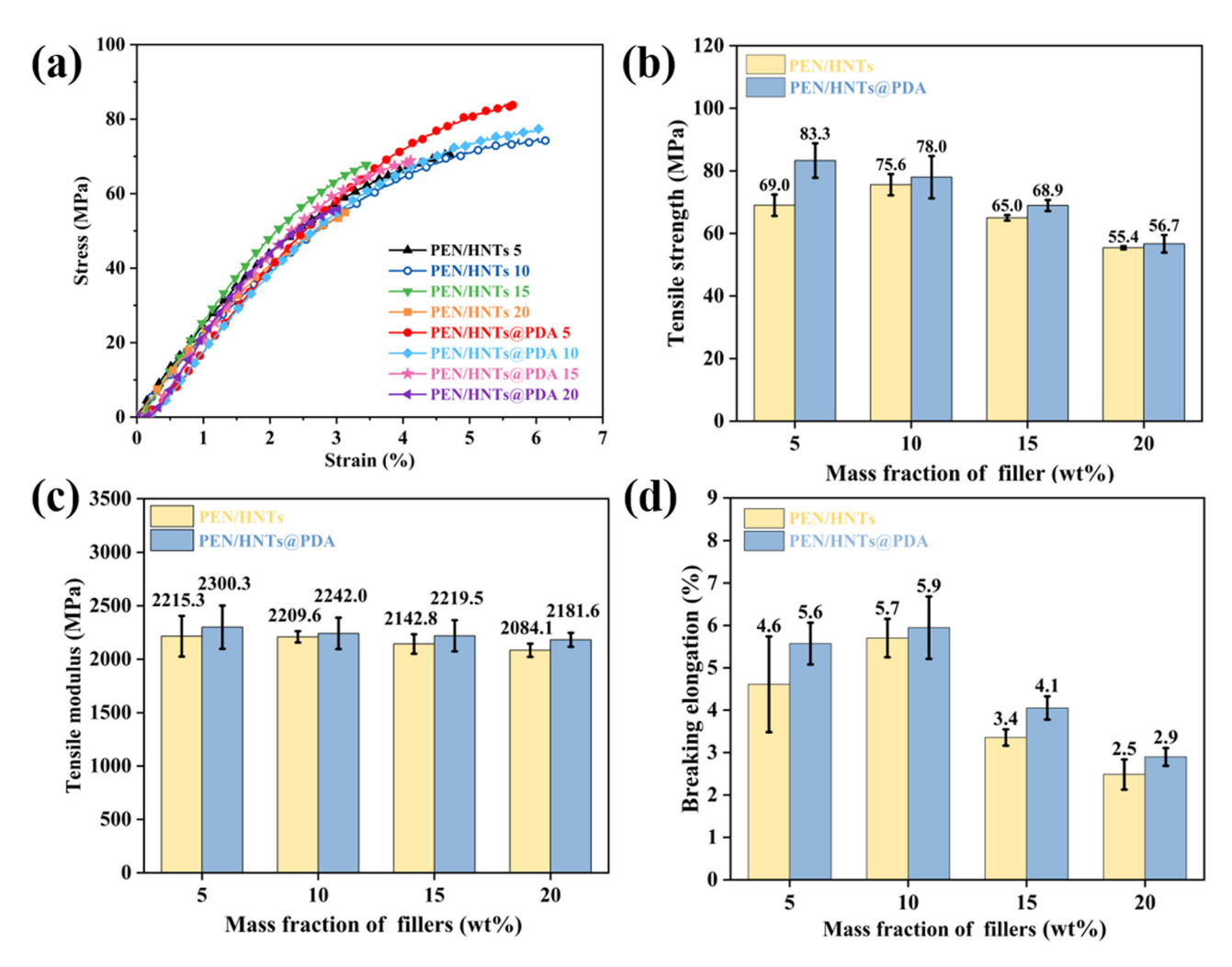


Figure 8: Mechanical properties of PEN composite films: (a) stress-strain curves; (b) tensile strength; (c) tensile modulus; and (d) elongation at break.

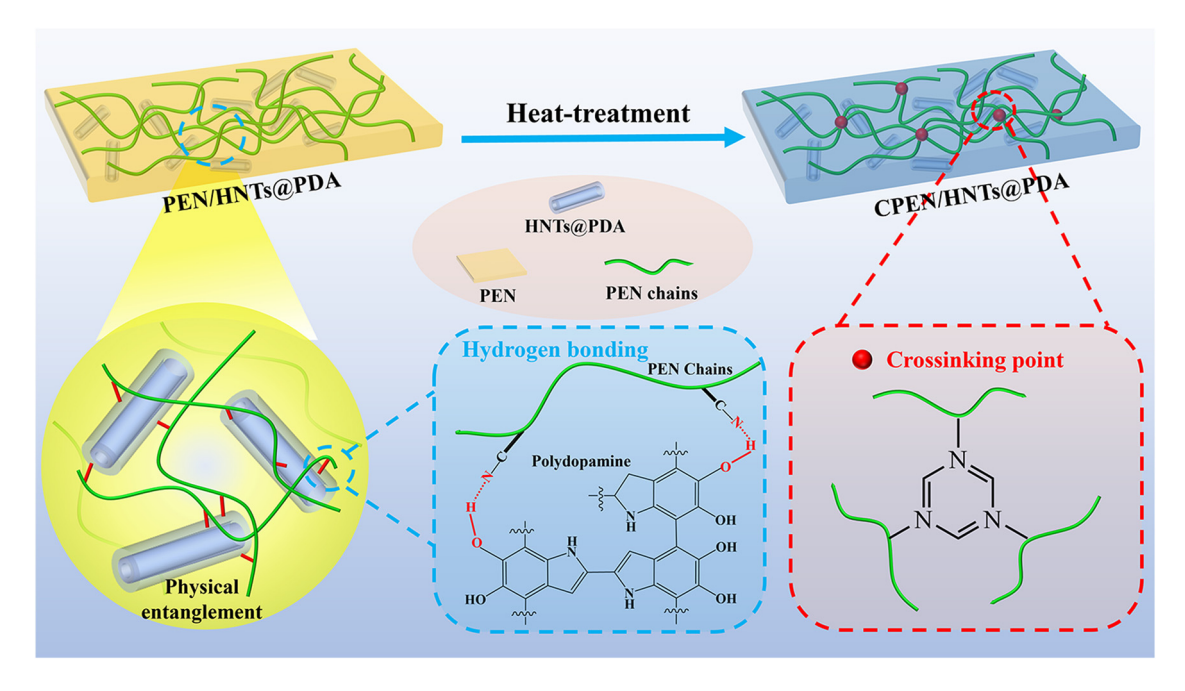


Figure 9: Schematic diagram of the internal structure before and after heat treatment of PEN nanocomposite film.

analyzed and are presented in Figure 8. By comparing with PEN/HNTs, the mechanical properties of PEN/HNTs@PDA composite films are significantly improved. This is mainly due to the following reasons: (1) the introduction of PDA makes HNTs@PDA hybrids have high repulsion and relatively small specific surface energy, which can be well dispersed in the polymer matrix, resulting in difficulty to agglomerate, and avoids pores and defects in the composite film; (2) the existence of PDA greatly improves the interface compatibility between the HNTs@PDA and the

PEN matrix, which further avoids the mechanical defects in the composite film; (3) the hydroxyl groups on the surface of PDA can form hydrogen bonds with the nitrile groups in the PEN molecular chain, thereby increasing the interaction of nanocomposites, and the corresponding mechanism diagram is shown in Figure 9. In summary, modification of HNTs with PDA can effectively enhance the mechanical properties of the PEN nanocomposites.

In addition, when pure PEN is subjected to high temperature heat treatment, its tensile modulus is further

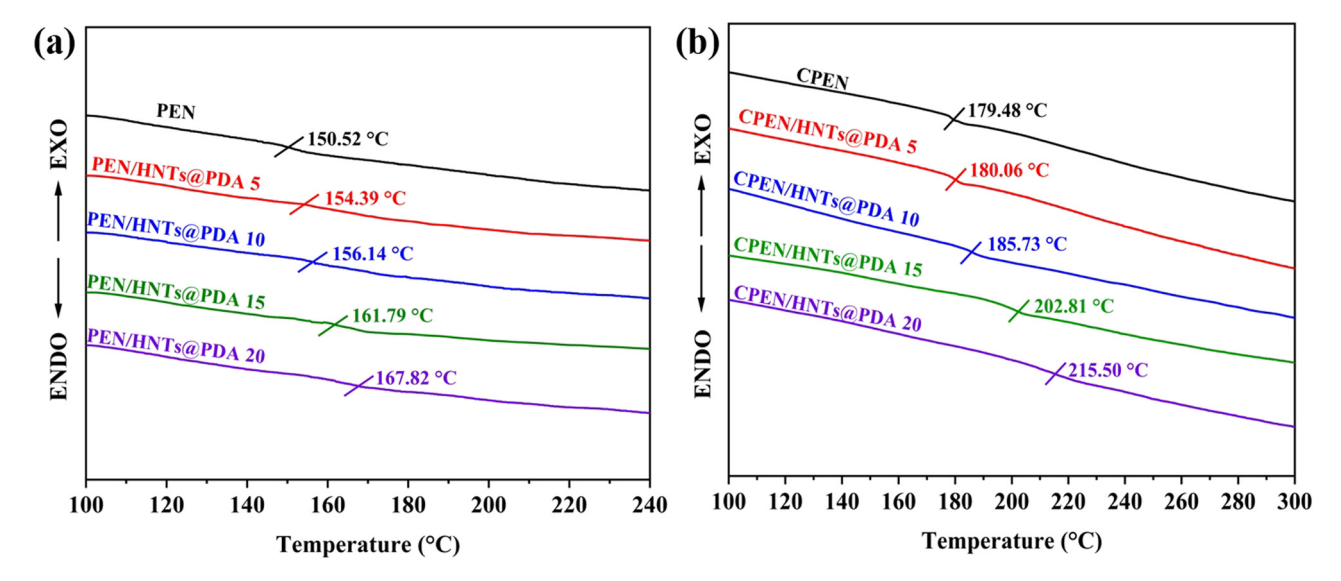


Figure 10: The DSC curves of composite films: (a) PEN/HNTs@PDA and (b) CPEN/HNTs@PDA.

improved, and the corresponding stress-strain curve is shown in Figure S3. This enhancement can primarily be attributed to the chemical reaction of the nitrile groups within the PEN molecular chain at elevated temperatures, leading to the formation of triazine rings and the establishment of a chemical cross-linking network. Figure 9 shows the schematic diagram of the corresponding mechanism, and the FTIR spectrum of PEN before and after the reaction is shown in Figure S4. It is clear that the peak of 2,240 cm⁻¹ belongs to the characteristic stretching band of the nitrile group. After heat treatment, it can be clearly seen from the CPEN curve that absorption peaks appear at 1.520 and 1,360 cm⁻¹, which are mainly specific absorption bands of triazine rings [30,31]. The results further confirm the production of triazine rings in CPEN films, resulting in the formation of a chemical cross-linking network inside its molecules.

In addition, the physical images of PEN composite films are shown in Figure S5. The PEN/HNTs@PDA composite film can be arbitrarily rolled into different shapes, even when the filler content is as high as 20%. In addition, even after the composite film is heat treated, CPEN/HNTs@PDA still retains excellent flexibility. Therefore, the abovementioned PEN nanocomposites have potential application prospects as the flexible electronic devices.

Figure 10(a) shows the effect of the variation in the mass fraction of functionalized HNTs filler on the glass transition temperature ($T_{\rm g}$) of the PEN nanocomposites. The $T_{\rm g}$ of the pure PEN is 150.5°C, and the thermal stability gradually increases with the increase in the mass fraction of HNTs@PDA from 154.4 to 167.8°C. This is because the HNTs@PDA filler is entangled with the PEN molecular

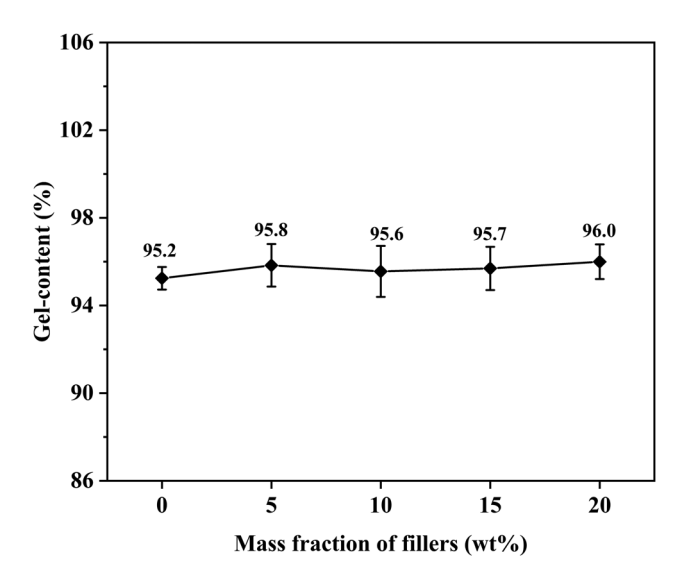


Figure 11: Gel content of CPEN/HNTs@PDA composite films.

chain in matrix resin and played a role in limiting the PEN molecular chain movement. In addition, the modification of filler facilitates the formation of a heat-resistant interface between the filler and the polymer matrix [32]. Herein, with the increase in the mass fraction of filler, the movement of polymer molecular chains is further restricted. Furthermore, the formation of hydroxyl groups on the PDA and nitrile groups on the PEN molecular chains makes the glass transition temperature to increase [33,34].

Meanwhile, the $T_{\rm g}$ of CPEN/HNTs@PDA composite dielectric films was characterized by DSC. As shown in Figure 10(b), the $T_{\rm g}$ of CPEN nanocomposites increased after high-temperature heat treatment, and $T_{\rm g}$ of CPEN/HNTs@PDA increased from 167.8 to 215.5°C. This result is due to the formation of triazine rings by the nitrile group between the PEN molecular chains, which further impede the movement of the molecular chains, resulting in a further increase in the $T_{\rm g}$ of the composite film [35,36], the corresponding internal mechanism diagram is shown in Figure 9.

To further investigate the degree of cross-linking of PEN nanocomposite films, in this work, the gel content of the nanocomposites was measured by Soxhlet extraction. The corresponding experimental methods and calculation formulas (equation S1) are listed in the supplementary information. As shown in Figure 11, the gel content of all nanocomposites is greater than 90%, which indicates that these films have a very high degree of cross-linking. This is due to the thermally induced self-cross-linking reaction of nitrile group on the PEN chain to form a triazine ring, producing cross-linked CPEN. This finding is consistent with the results obtained from the DSC tests [30,31].

Figure 12(a1-e1) shows the center-temperature of the PEN composite films filled with different HNTs@PDA contents after 10 s of laser irradiation. As the filler increases, the thermal conductivity of the composite films becomes more pronounced and the central temperature of the films gradually increases up to 49.7°C for PEN/HNTs@PDA 20. This is due to the gradual introduction of the HNTs ceramic filler, which promotes the thermal conductivity of the composite. Meanwhile, Figure 12(a2-e2) shows the center-temperature of the CPEN composite films after 10 s of laser irradiation. The center-temperature of all CPEN nanocomposites is higher than that of PEN nanocomposites, which is due to the formation of a triazine ring by the nitrile group between PEN molecular chains and the formation of hydrogen bonds between the hydroxyl groups on the PDA and the nitrile groups on the PEN molecular chains, which enhances the interfacial forces and promotes the further improvement of the thermal conductivity of the nanocomposites [37].

DE GRUYTER

Figure 13(a) shows the dielectric constant of the PEN/HNTs@PDA nanocomposites at room temperature, from which it can be observed that the change in dielectric constant with frequency is relatively stable for pure PEN film. It exhibits good dielectric properties-frequency stability. when the filler content is greater than 10 wt%, the dielectric constant of nanocomposites appears to be significantly improved. As can be found in Figure 13(a) and Figure S6(a),

compared with the pure PEN film (3.6 at 1 kHz), the dielectric constants of the nanocomposites are 8.6 and 11.6 (1 kHz) when the HNTs@PDA content is 15 and 20 wt%, respectively, which are 2.4 and 3.2 times larger than pure PEN. And the change in dielectric constant with frequency gradually increases, the dielectric constant-frequency stability gradually decreases. This is due to the large specific surface area of HNTs, which is conducive to the formation

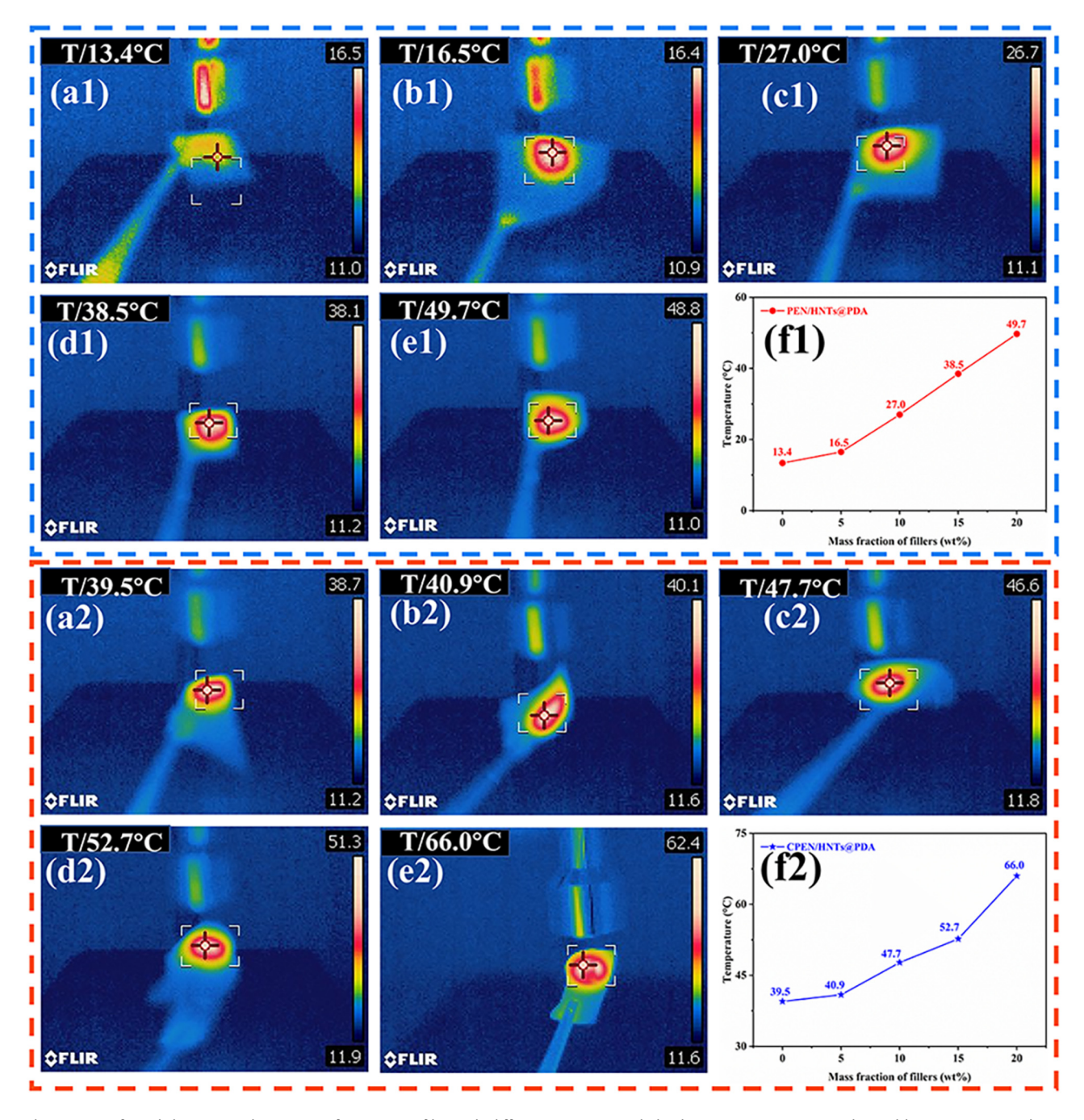


Figure 12: Infrared thermographic image of composite film with different HNTs@PDA hybrids: (a1) PEN; (a2) CPEN; (b1 and b2) 5 wt%; (c1 and c2) 10 wt%; (d1 and d2) 15 wt%; (e1 and e2) 20 wt%; (f1 and f2) the center-temperature of nanocomposites;.

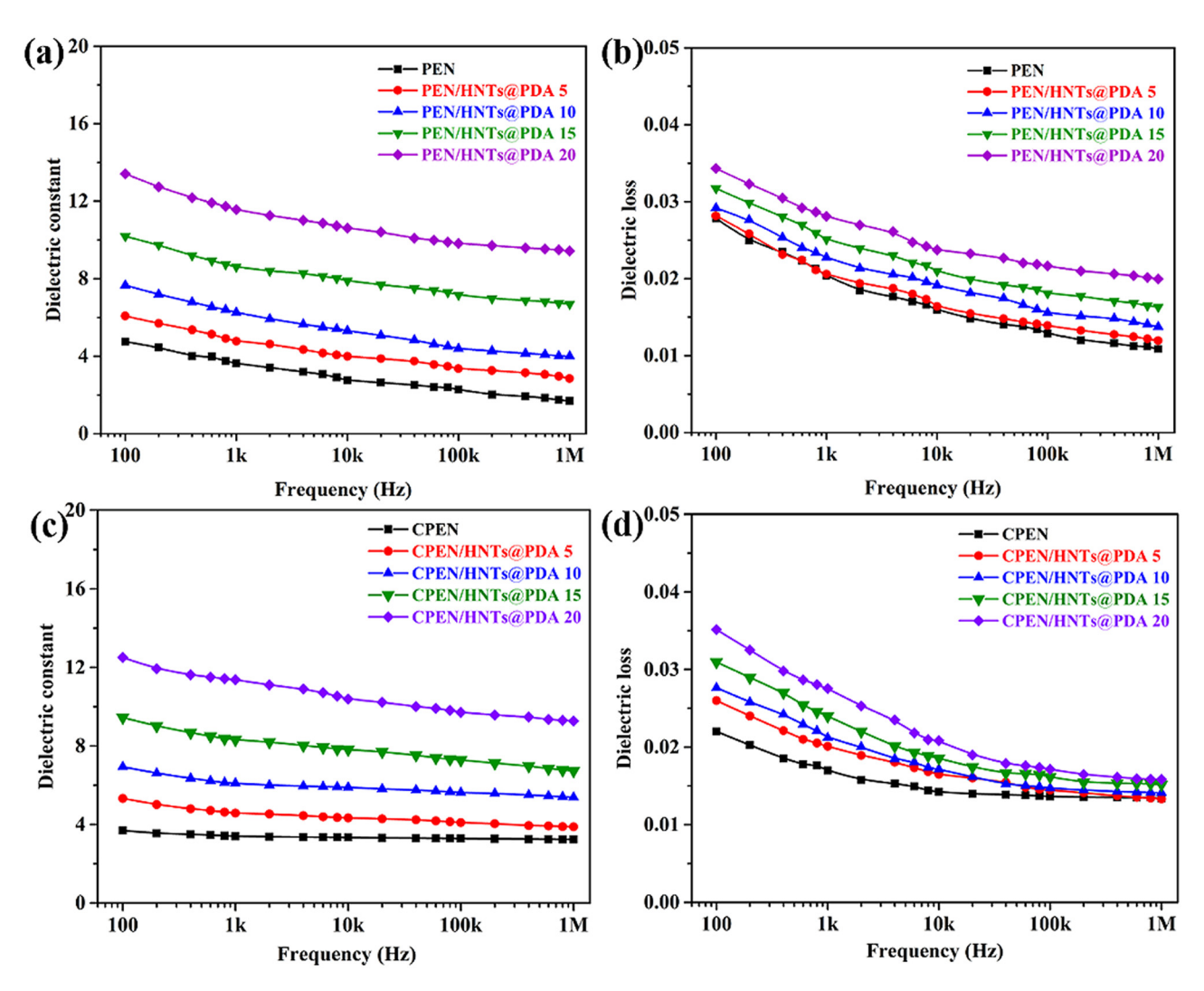


Figure 13: Dielectric properties of nanocomposite films: (a) and (b) PEN/HNTs@PDA and (c) and (d) CPEN/HNTs@PDA.

of micro-capacitance inside the PEN matrix and the formation of Maxwell–Wagner–Sillars polarization with high intensity with the applied electric field [38,39]. Therefore, the dielectric constants of the nanocomposites are greatly enhanced. In addition, the dielectric constant gradually decreases with the increase in the test frequency, which is because the polarization speed in the system cannot keep up with the electric field frequency change, resulting in the polarization hysteresis phenomenon [40–42].

Meanwhile, Figure 13(b) and Figure S6(b) show the dielectric loss–frequency curves of the PEN/HNTs@PDA nanocomposite films. With the rise of filler content, the dielectric loss of films gradually increases. However, the dielectric loss of several nanocomposites with different contents is less than 0.03, remaining at a relatively low level, which can be well applied to practical production [43]. As shown in Figure 13(c) and (d) and Figure S6(c) and (d), on

comparing with the PEN/HNTs@PDA composite films, the dielectric properties-frequency of CPEN/HNTs@PDA are more stable, which is mainly attributed to the formation of cross-linking network, which hinders the movement of molecular chains and reduces the internal polarization of molecules. In addition, the hydrogen bond formed between the HNTs@PDA and the PEN matrix reduces the interfacial polarization of the system. Therefore, the dielectric performance-frequency relationship of CPEN composite film is more stable.

Figure 14 shows the dielectric performance–temperature relationship curves of the composite films, from which it can be seen that when the temperature is below the $T_{\rm g}$ of the nanocomposites, their dielectric constant remains stable. However, when the temperature exceeds the $T_{\rm g}$ the dielectric constant increases sharply. Usually, when the test temperature exceeds the $T_{\rm g}$ of the composite film, the polymer molecular chain begins to move violently, and

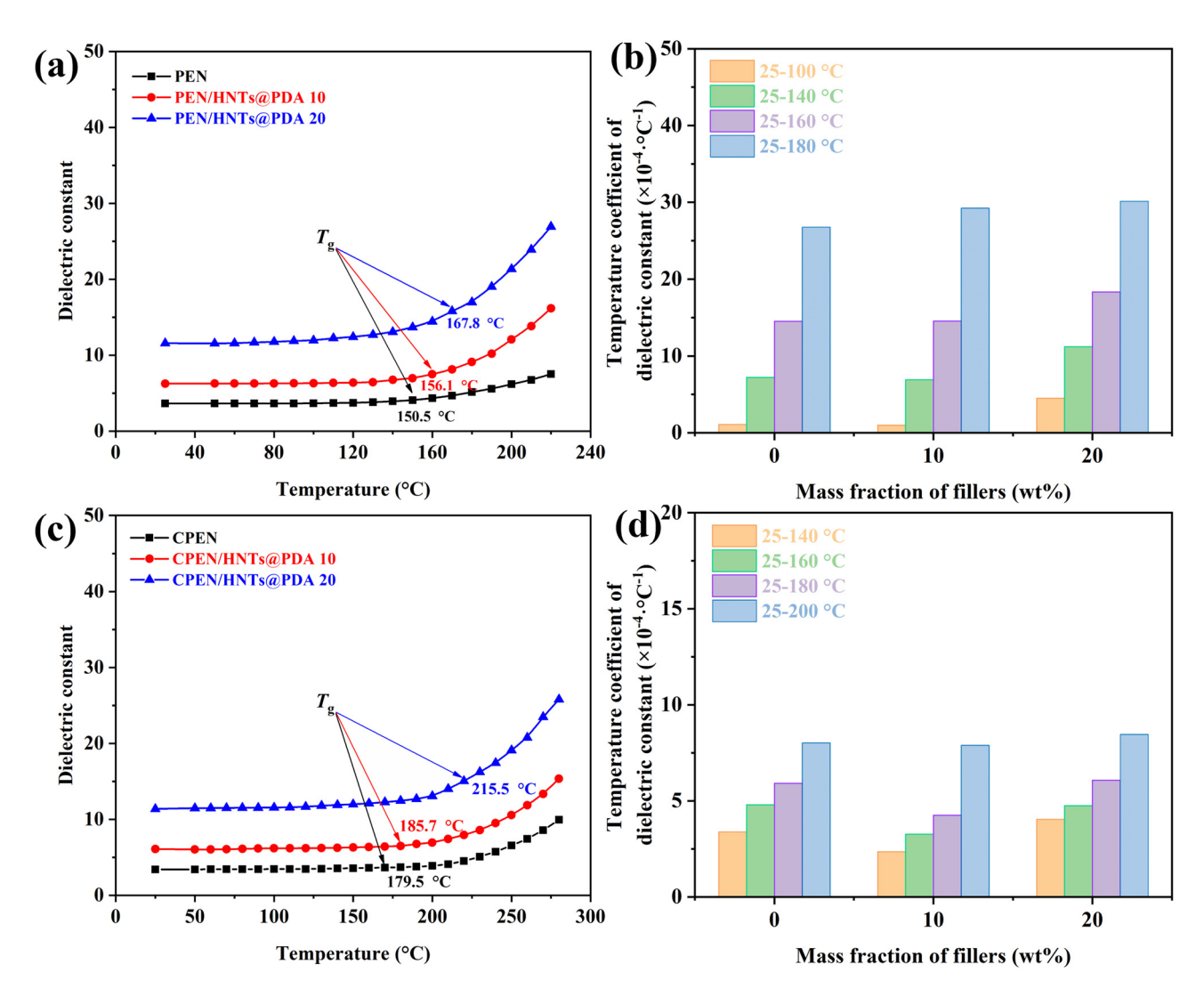


Figure 14: Dielectric properties of composite films: (a) and (c) temperature-permittivity relationship diagram and (b) and (d) dielectric constant-temperature coefficient.

the movement of the free charge inside the molecule intensifies. Therefore, the polarization effect inside the composite film increases, and the macroscopic manifestation is a sharp

increase in the dielectric constant [44,45]. Another phenomenon is that the dielectric constant-temperature stability of CPEN/HNTs@PDA nanocomposites is significantly better

Table 1: Comparison of dielectric properties of different composite dielectric materials

Samples	Content (%)	Dielectric constant (1 kHz)	Dielectric loss (1 kHz)	Working temperature (°C)	Ref.
PLA/HNTs	10	0.26	~1.480	62.2	[47]
PEDOT/PVDF-HNTs	7	~75	~0.150	160.0	[48]
IPTS/SiR-HNTs	9	~6.2	~0.070	_	[49]
P(VDF-CTFE)/HNTs	5	~18	~0.054	_	[11]
PC/HNTs	6	~3.7	0.118	_	[50]
PVB/HNTs	10	~3.8	~0.030	_	[51]
PI/HNTs	10	~3.8	~0.010	_	[52]
PEN/HNTs@PDA	10	6.26	0.022	~160	This work
CPEN/HNTs@PDA	10	6.10	0.021	~180	This work

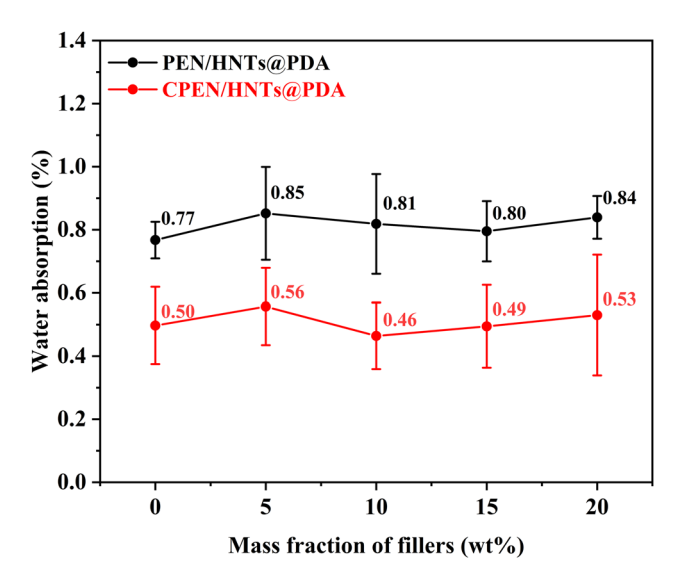


Figure 15: Water absorption of composite films.

than that of PEN/HNTs@PDA (Figure 14(a) and (c)). This is mainly because after heat treatment, a triazine ring is generated inside the CPEN/HNTs@PDA composite films, forming a large number of cross-linked networks, thereby obtaining higher $T_{\rm g}$. Therefore, the CPEN composite films have better dielectric properties-temperature stability [30,46].

In addition, the dielectric constant-temperature coefficient is calculated by equation S2 [46]. The final calculated results are shown in Figure 14(b) and (d). It is clear that when the test temperature is from 25 to 160°C, the dielectric constant-temperature coefficient of the nanocomposite film is lower than 2×10^{-3} ° C⁻¹, indicating that the composite film has good dielectric constant-temperature coefficient stability in this temperature range. However, when the temperature exceeds 160°C, the dielectric constant-temperature coefficient increases significantly. Comparing the results of PEN/HNTs@PDA with CPEN/HNTs@PDA, it is observed that the dielectric constant-temperature coefficient of CPEN/HNTs@PDA composite films remains consistently low within the temperature range of 25-180°C, all being less than 7×10^{-4} ° C⁻¹ (Figure 14(c) and (d) and Figure S7). This is because the cross-linking network inside the CPEN composite film greatly restricts the movement of the CPEN molecular segment, so all CPEN composite films have better temperature coefficient and dielectric constant. This result confirms that the CPEN composite film has excellent dielectric stability at high temperature, which means that it can be used in practical applications at 180°C.

Moreover, to further clearly demonstrate the performance of CPEN/HNTs@PDA nanocomposites, the dielectric properties and working temperature of different nanocomposites containing HNTs at room temperature are summarized

in Table 1. Among them, most nanocomposites have a dielectric constant lower than 5, and the working temperature of PLA/HNTs, PEDOT/PVDF-HNTs, and Epoxy/m-HNTs is less than 160°C. In comparison, the CPEN/HNTs@PDA nanocomposites in this work has a high dielectric constant and a very low dielectric loss, and it can be used as dielectric films in environments with the working temperatures up to 180°C.

Figure 15 shows the water absorption rate of composite films with different filler contents, and the corresponding calculation formula (equation S3) is listed in the supplementary information. The results show that the water absorption rate of all nanocomposites is less than 0.9%. Owing to the nitrile group in the PEN molecular chain, the PEN composite film has good hydrophobicity. After high temperature heat treatment, the PEN molecular chains are cross-linked with each other to form a cross-linking network, resulting in lower water absorption of CPEN composite films [35]. This result provides a theoretical basis for the application of this kind of composite film in various electronic and electrical fields [36,53,54].

4 Conclusion

In conclusion, this work develops a straightforward method to prepare PEN nanocomposites. The HNTs were coated by PDA through in situ polymerization to form a core-shell structure HNTs@PDA, which were then introduced into the PEN matrix as functional fillers. The hydrogen bond formed between the nitrile group and hydroxyl group improves the interface interaction between the HNTs@PDA and the PEN matrix, which makes the PEN/HNTs@PDA nanocomposites have good interfacial compatibility, and mechanical and dielectric properties. When the filler content is 5 wt%, the tensile strength and modulus of the composite film reach 83.3 and 2300.3 MPa, respectively, which is much higher than that of PEN. Besides, dielectric constant of PEN/ HNTs@PDA 20 is 11.56 at 1 kHz. In addition, after hightemperature heat treatment, a chemical cross-linking reaction occurred within the PEN matrix, further enhancing the thermal stability of the nanocomposite films. The results show that the $T_{\rm g}$ of CPEN/HNTs@PDA 20 composite film reaches 215.5°C, which is 47.7°C higher than that of PEN/ HNTs@PDA 20. Furthermore, the dielectric constant-temperature coefficient of all CPEN composite films is less than $7 \times 10^{-4} \,^{\circ}\text{C}^{-1}$ at the temperature range of 25–180°C. Overall, this work provides a simple and environmentally friendly approach for the fabrication of high-performance composite dielectric films suitable for organic film capacitors.

Funding information: This work was supported by National Natural Science Foundation of China (No. 52203102), the Natural Science Foundation of Sichuan Province (2022NSFSC2009), the Fundamental Research Funds for the Central Universities, Southwest Minzu University (ZYN2023096), and the Science and Technology Planning Project of Longquanyi, Chengdu (No. LQXKJ-KJXM-2022-04).

Author contributions: All authors have accepted responsibility for the entire content of this manuscript and approved its submission.

Conflict of interest: The authors state no conflict of interest.

References

- [1] Hamciuc C, Lisa G, Serbezeanu D, Gradinaru LM, Asandulesa M, Tudorachi N, et al. Tailoring thermal and electrical properties of Jeffamine segmented polyetherimide composite films containing BaTiO₃ particles. Polymers. 2022;14(21):4715.
- [2] Beak K, Choi M, Kim DH, Yu Y, Theerthagiri J, Al-Mohaimeed AM, et al. Silane-treated BaTiO₃ ceramic powders for multilayer ceramic capacitor with enhanced dielectric properties. Chemosphere. 2022;286:131734.
- [3] Wang HY, Cao MH, Mao TL, Fu JQ, Pan WG, Hao H, et al. Fabrication of BaTiO₃@FeO core-shell nanoceramics for dielectric capacitor applications. Scr Mater. 2021;196:113753.
- [4] Cheng C, Song WH, Zhao Q, Zhang HL. Halloysite nanotubes in polymer science: purification, characterization, modification and applications. Nanotechnol Rev. 2020;9(1):323–44.
- [5] Cavallaro G, Milioto S, Lazzara G. Halloysite nanotubes: interfacial properties and applications in cultural heritage. Langmuir. 2020;36(14):3677–89.
- [6] Du ML, Guo BC, Jia DM. Newly emerging applications of halloysite nanotubes: A review. Polym Int. 2010;59(5):574–82.
- [7] Chen XX, Li Y, Wang Y, Song DQ, Zhou ZW, Hui D. An approach to effectively improve the interfacial bonding of nano-perfused composites by *in situ* growth of CNTs. Nanotechnol Rev. 2021;10(1):282–91.
- [8] Tang HL, Wang P, Zheng PL, Liu XB. Core-shell structured BaTiO₃@polymer hybrid nanofiller for poly(arylene ether nitrile) nanocomposites with enhanced dielectric properties and high thermal stability. Compos Sci Technol. 2016;123:134–42.
- [9] Ran QM, Fan ZL, Guo XK, Li XL, Yi KY, Liu XB, et al. Simultaneous adsorption and fluorescent detection of Cr(vi) via lanthanide coordinating polymeric porous microparticles. Chem Eng J. 2023;457:141214.
- [10] Yang JY, Tang ZL, Yin H, Liu Y, Wang L, Tang HL, et al. Poly(arylene ether nitrile) composites with surface-hydroxylated calcium copper titanate particles for high-temperature-resistant dielectric applications. Polymers. 2019;11(5):766.
- [11] Ye HJ, Wang QP, Sun Q, Xu LX. High energy density and interfacial polarization in poly(vinylidene fluoride-chlorotrifluoroethylene) nanocomposite incorporated with halloysite nanotube architecture. Colloid Surf A. 2020;606:125495.

- [12] Tarawneh MA, Saraireh SA, Chen RS, Ahmad SH, Al-Tarawni MM, Yu LJ, et al. Mechanical reinforcement with enhanced electrical and heat conduction of epoxy resin by polyaniline and graphene nanoplatelets. Nanotechnol Rev. 2020;9(1):1550–61.
- [13] Zeng JJ, Tang JY, Jin TT, Pu LY, Wei XH, Huang X, et al. Enhanced energy density of poly(arylene ether nitriles) composites filled with surface engineered BaTiO₃ nanoparticles. Sensor Actuat A-Phys. 2020:315:112185.
- [14] Song Y, Ye G, Wu FC, Wang Z, Liu SY, Kopeć M, et al. Bioinspired polydopamine (PDA) chemistry meets ordered mesoporous carbons (OMCs): a benign surface modification strategy for versatile functionalization. Chem Mater. 2016;28:5013–21.
- [15] Qiu WZ, Yang HC, Xu ZK. Dopamine-assisted co-deposition: an emerging and promising strategy for surface modification. Adv Colloid Interface Sci. 2018;256:111–25.
- [16] Cheng W, Zeng XW, Chen HZ, Li ZM, Zeng WF, Mei L, et al. Versatile polydopamine platforms: synthesis and promising applications for surface modification and advanced nanomedicine. Acs Nano. 2019;13(8):8537–65.
- [17] Tang HL, Yang J, Zhong JC, Zhao R, Liu XB. Synthesis and dielectric properties of polyarylene ether nitriles with high thermal stability and high mechanical strength. Mater Lett. 2011;65:2758–61.
- [18] Wan XY, Zhan YQ, Zeng GY, He Y. Nitrile functionalized halloysite nanotubes/poly(arylene ether nitrile) nanocomposites: Interface control, characterization, and improved properties. Appl Surf Sci. 2017;393:1–10.
- [19] Ma R, Yang PB, Ma Y, Bian FL. Facile synthesis of magnetic hierarchical core-shell structured ${\rm Fe_3O_4@PDA-Pd@MOF}$ nanocomposites: highly integrated multifunctional catalysts. Chemcatchem. 2018;10(6):1446–54.
- [20] Qu Y, Qin L, Guo MC, Liu XG, Yang YZ. Multilayered molecularly imprinted composite membrane based on porous carbon nanospheres/PDA cooperative structure for selective adsorption and separation of phenol. Sep Purif Technol. 2022;280:119915.
- [21] Mishra G, Mukhopadhyay M. TiO₂ decorated functionalized halloysite nanotubes (TiO₂@HNTs) and photocatalytic PVC membranes synthesis, characterization and its application in water treatment. Sci Rep. 2019;9(1):4345.
- [22] Li L, Lu LM, Wu SQ, Hu DY, Tang TY, Tang YL. Study on spectral properties of butyl hydroxytoluene: experiment and theoretical calculation. Inorg Chem Commun. 2023;148:110283.
- [23] Zhao L, Bi DD, Qi XY, Guo YF, Yue F, Wang XT, et al. Polydopamine-based surface modification of paclitaxel nanoparticles for osteo-sarcoma targeted therapy. Nanotechnology. 2019;30(25):255101.
- [24] Shankar S, Kasapis S, Rhim JW. Alginate-based nanocomposite films reinforced with halloysite nanotubes functionalized by alkali treatment and zinc oxide nanoparticles. Int J Biol Macromol. 2018;118:1824–32.
- [25] Zhou XS, Jin B, Luo J, Xu XY, Zhang LL, Li JJ, et al. Dramatic visible light photocatalytic degradation due to the synergetic effects of TiO₂ and PDA nanospheres. RSC Adv. 2016;6(69):64446–9.
- [26] Luo RF, Tang LL, Zhong S, Yang ZL, Wang J, Weng YJ, et al. *In vitro* investigation of enhanced hemocompatibility and endothelial cell proliferation associated with quinone-rich polydopamine coating. ACS Appl Mater Interfaces. 2013;5(5):1704–14.
- [27] Wang YJ, Kai Y, Tong LF, You Y, Huang YM, Liu XB. The frequency independent functionalized MoS₂ nanosheet/poly(arylene ether nitrile) composites with improved dielectric and thermal properties via mussel inspired surface chemistry. Appl Surf Sci. 2019;481:1239–48.

- [28] Tong LF, He L, Zhan CH, Xia YQ, Liu XB. Poly(arylene ether nitrile) dielectric film modified by Bi₂S₃/rGO-CN fillers for high temperature resistant electronics fields. Chin J Polym Sci. 2022;40(11):1441-50.
- [29] Yuan H, Liu XH, Ma LM, Yang ZG, Wang HG, Wang JQ, et al. Application of two-dimensional MoS₂ nanosheets in the property improvement of polyimide matrix: mechanical and thermal aspects. Compos Part A. 2017;95:220-8.
- [30] Paul B, Bailly L, Beque D, Lartigau-Dagron C, Hassoune-Rhabbour B, Nassiet V. Thermal degradation mechanisms of the cured phenolic triazine thermoset resin (PT30) studied under nitrogen. Polym Degrad Stab. 2023;208:110250.
- [31] Ariraman M, Sasikumar R, Alagar M. Shape memory effect on the formation of oxazoline and triazine rings of BCC/DGEBA copolymer. Rsc Adv. 2015;5(85):69720-7.
- [32] Wang J, Li Z, Yan Y, Wang X, Xie YC, Zhang ZC. Improving ferro- and piezo- electric properties of hydrogenized poly(vinylidene fluoridetrifluoroethylene) films by annealing at elevated temperatures. Chinese | Polym Sci. 2016;34(5):649-58.
- [33] Zhu Y, Luo YM, Tang XR, Tong LF, Liu XB. Enhanced thermal conductivity of polyarylene ether nitrile composites blending hexagonal boron nitride. J Appl Polym Sci. 2023;140(10):e53597.
- [34] Zhang C, Dai XY, Xing ZL, Guo SW, Li F, Chen X, et al. Investigation on the structure and performance of polypropylene sheets and biaxially oriented polypropylene films for capacitors. Chin J Polym Sci. 2022;40(12):1688-96.
- [35] Feng MN, Ma DY, Chen XR, Wang P, Lin J. Enhanced dielectric properties of poly(arylene ether nitrile) composite films employing MoS₂-based semiconductors for organic film capacitor applications. Mat Sci Semicon Proc. 2021;136:106127.
- [36] He L, Tong LF, Bai ZX, Lin G, Xia YQ, Liu XB. Investigation of the controllable thermal curing reaction for ultrahigh T_{α} polyarylene ether nitrile compositions. Polymer. 2022;254:125064.
- [37] Yang W, Zhan YO, Feng QY, Sun A, Dong HY. Flexible h-BN/fluorinated poly (arylene ether nitrile) fibrous composite film with low dielectric constant and high thermal conductivity fabricated via coaxial electrospinning hot-pressing technique. Colloid Surf A. 2022;649:129455.
- [38] Tian G, Deng W, Xiong D, Yang T, Zhang BB, Ren XR, et al. Dielectric micro-capacitance for enhancing piezoelectricity via aligning MXene sheets in composites. Cell Rep Phys Sci. 2022;3(4):100814.
- [39] Redhu P, Sharma P, Hooda A, Singh A, Ohlan A, Punia R. Correlation of dielectric, ferroelectric, and magnetic properties with structural changes in Cr doped BCT ceramics. Appl Phys A-Mater. 2023;129(7):523.
- [40] Zhang JJ, Li HR, Hu D, Fang D, Luo ZP, Tu JY, et al. A new strategy for the preparation of silver/epoxy/poly(vinylidene fluoride) dielectric composites with a multi-interface structure for suppressed dielectric loss. Polym Compos. 2018;39:E2606-10.
- [41] Luo HB, Pan XR, Yang JH, Qi XD, Wang Y. Simultaneously improved dielectric constant and breakdown strength of PVDF-based com-

- posites with polypyrrole nanowire encapsuled molybdenum disulfide nanosheets. Chin J Polym Sci. 2022;40(5):515-25.
- [42] Zhan JY, Tian GF, Wu ZP, Qi SL, Wu DZ. Preparation of polyimide/ BaTiO₃/Ag nanocomposite films via in situ technique and study of their dielectric behavior. Chin J Polym Sci. 2014;32(4):424-31.
- [43] Chen SJ, Ren DX, Li B, Xu MZ, Liu XB. Investigation on phenolphthalein and bisphenol AF based poly(arylene ether nitrile) copolymers: preparation, thermal, mechanical and dielectric properties. Polym Test. 2021;96:107091.
- [44] Zhan YQ, Yang J, Zhou YK, Yang XL, Meng FB, Liu XB. Nitrile functionalized graphene for poly(arylene ether nitrite) nanocomposite films with enhanced dielectric permittivity. Mater Lett.
- [45] Li Q, Chen L, Gadinski MR, Zhang SH, Zhang GZ, Li HU, et al. Flexible high-temperature dielectric materials from polymer nanocomposites. Nature. 2015;523:576-9.
- [46] You Y, Liu SN, Tu L, Wang YJ, Zhan CH, Du XY, et al. Controllable fabrication of poly(arylene ether nitrile) dielectrics for thermalresistant film capacitors. Macromolecules. 2019;52(15):5850-9.
- [47] Rajan KP, Al-Ghamdi A, Thomas SP, Gopanna A, Chavali M. Dielectric analysis of polypropylene (PP) and polylactic acid (PLA) blends reinforced with halloysite nanotubes. J Thermoplast Compos. 2018;31(8):1042-53.
- [48] Wang F, Zhang XH, Ma YH, Chen D, Yang WT. Conductive HNTs-PEDOT hybrid preparation and its application in enhancing the dielectric permittivity of HNTs-PEDOT/PVDF composites. Appl Surf Sci. 2018;458:924-30.
- [49] Wang RL, Wang Y, Liang YF, Yang Z, Bai YP, He JM. Insights into the synergistic effect of methoxy functionalized halloysite nanotubes for dielectric elastomer with improved dielectric properties and actuated strain. Compos Sci Technol. 2023;231:109802.
- Santhosh G, Nayaka GP, Aranha J, Siddaramaiah. Investigation on electrical and dielectric behaviour of halloysite nanotube incorporated polycarbonate nanocomposite films. Trans Indian Inst Met. 2017;70(3):549-55.
- [51] Su YT, Zhou MP, Sui G, Lan JL, Zhang HT, Yang XP. Polyvinyl butyral composites containing halloysite nanotubes/reduced graphene oxide with high dielectric constant and low loss. Chem Eng J. 2020;394:124910.
- [52] Zhu TW, Qian C, Zheng WW, Bei RX, Liu SW, Chi ZG, et al. Modified halloysite nanotube filled polyimide composites for film capacitors: high dielectric constant, low dielectric loss and excellent heat resistance. RSC Adv. 2018;8(19):10522-31.
- [53] Yang J, Yang XL, Zhan YQ, Zou YK, Zhao R, Liu XB. Synthesis and properties of cross-linked poly(arylene ether nitriles) containing pendant phthalonitrile. J Appl Polym Sci. 2013;127(3):1676-82.
- Cao T, Shi Y, Li X, Peng J, Liu X, Huang Y. Dual cross-linking strategy [54] to prepare fluorine-containing poly(arylene ether nitrile) films with a low dielectric constant and ultra-low water uptake. Polym Chem. 2022;13(44):6213-22.